TWO-DIMENSIONAL WRINKLE RIDGE STRAIN & ENERGY RELEASE BASED ON NUMERICAL MODELING OF MOLA TOPOGRAPHY. C. H. Okubo[1] and R. A. Schultz, Geomechanics-Rock Fracture Group, Department of Geological Sciences/172, Mackay School of Mines, University of Nevada, Reno, NV, 89557-0138. [1]chriso@mines.unr.edu.

Introduction: Wrinkle ridges are fault-related folds [1,2]. Geologic strain accommodated across a wrinkle ridge is manifest as brittle slip along subjacent thrust faults, as well as folding of the surrounding rock mass. Therefore, quantifying 2-D wrinkle ridge strain and energy release requires measurement of both the strain accommodated by faults and the strain accommodated by folding of the surrounding crust.

Wrinkle ridge topography is commonly used to evaluate strain at the *uppermost surface* of the crust using analytical techniques of unrolling [3,4,5], kinematics [6], and displacement-length scaling [7]. The depth-dependent distribution of shear strain along the thrust faults and the volumetric strain between wrinkle ridges, however, has largely remained unaddressed.

In this abstract, we use numerical models of MOLA-based wrinkle ridge topography to determine fault-induced displacement vectors of the subjacent crust. These displacements not only provide individual magnitudes of fault- and fold-related strain, but more significantly provide a measurement of the work done, or energy released, through wrinkle ridge formation.

Methods: A boundary element model [8] is used to calculate the distribution of slip along model thrust fault geometries, as well as attendant displacement vectors within the surrounding crust, based on a prescribed remote stress state and crustal strength distribution. Resulting model surface displacements are compared to cross-strike wrinkle ridge topographic profiles. The model thrust fault geometry is iteratively varied until model surface displacements fit the MOLA topography. In this way, the best-fit fault geometry yields 2-D (plane strain) distributions of fault slip and material displacements consistent with observed topography. Model displacement vectors along the fault and within the surrounding material are then used to calculate values of fault shear strain, as well as horizontal and vertical normal strain within the surrounding crust. Finally, material displacements are used to calculate the work done (in joules) by faulting and by faulting & folding.

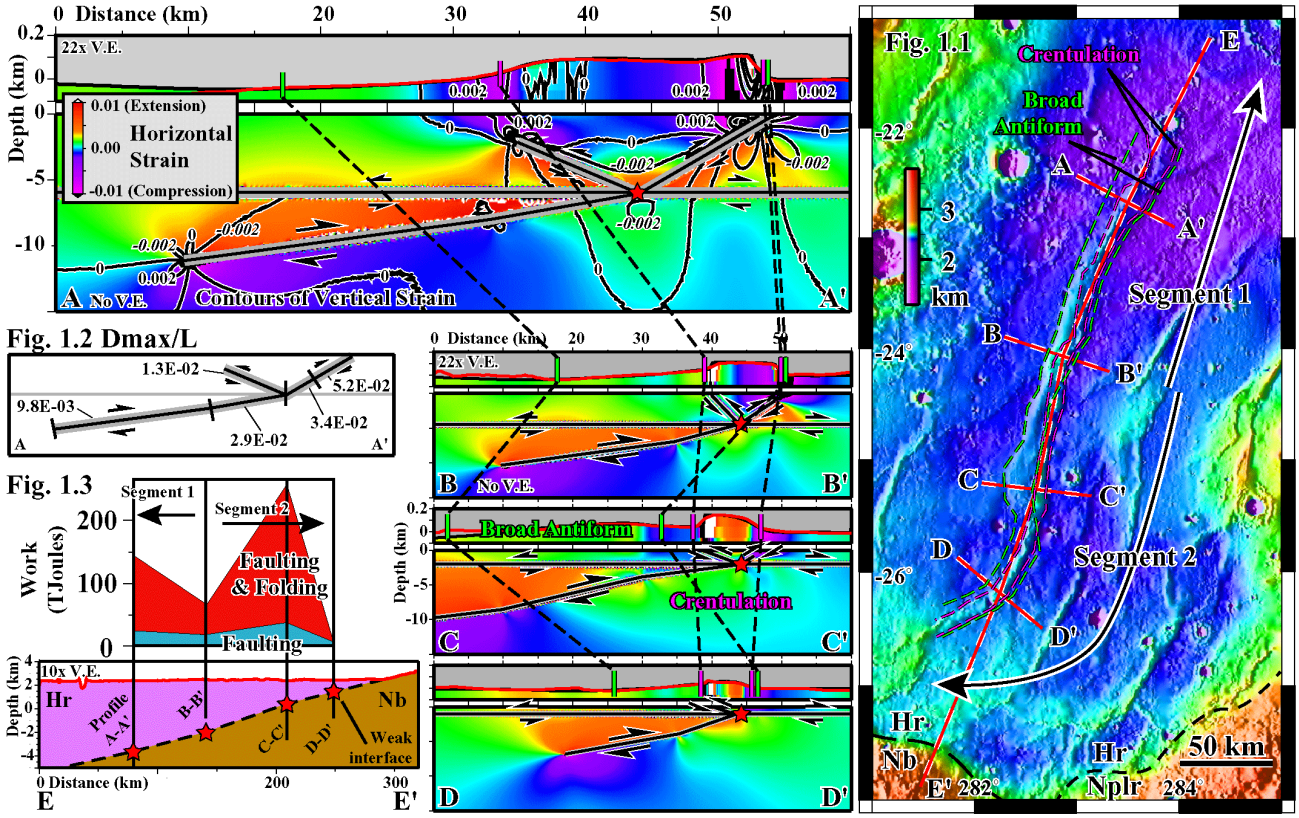

Figure 1. Depth-dependent strain and fault geometry across a Solis Planum wrinkle ridge based on numerical modeling of MOLA topography. 1.1) Color-as-height MOLA DEM showing the locations of model strain profiles A–D. Color in profiles A–D represent horizontal normal strain, and contours in A are vertical normal strain. 1.2) Brittle shear strain across faults in A. 1.3) Work done by faulting (blue) and work done by faulting & folding (red) along each profile. Local minima in work done define wrinkle ridge segments. Nb/Hr profile E based on weak horizon depths (stars) of A–D.

The distribution of layer or interface strength within the crust strongly influences the propagation path of thrust faults and thereby effects the distribution of strain and energy release. Mechanically weak horizons impede up-dip propagation of thrust faults [9,10] and lead to nucleation of secondary faults, specifically backthrusts above the intersection of the weak horizon and the primary thrust [11]. Without weak horizons, a thrust fault can propagate unimpeded to the surface, and, significantly, the formation of backthrusts is not predicted. Thus, where our models indicate the presence of a backthrust, we prescribe a horizontal weak horizon at the depth of the primary thrust and backthrust intersection.

Results: Figure 1 shows four cross-strike MOLA-based topographic profiles along a wrinkle ridge in Solis Planum, with corresponding best-fit fault geometries and predictive maps of normal strain. The northern terminus of the ridge has the classic wrinkle ridge profile of a narrow, high-amplitude crenulation superimposed upon a broader antiform [1,4,5], while the southern terminus resembles the broad antiform of a lobate scarp [12].

Our results show that the narrow crenulation on this wrinkle ridge is the surface expression of a fold surrounding a backthrust and the upper tip of the primary thrust, and that the broader antiform is the expression of a fold around the deeper sections of that primary thrust. All our profiles show evidence of a weak interface that is deepest at A–A' and shallows toward D–D' (see E-E'). This interface may represent the contact between the Hesperian ridged plains material (Hr) and Noachian basement complex (Nb) of [13].

The narrow crenulation has been previously observed to 'wander' along-strike of wrinkle ridges from one side of the broad antiform to the other [14,15]. Our results show that this may be due variability in depth to a subjacent weak horizon, as well as changes in fault dip and length. Additionally, wrinkle ridge to lobate scarp transitions [16,17] may be due to a progressive shallowing of a weak horizon or to a decrease in the strength contrast between that horizon and the surrounding crust.

Cumulative surface strain across each wrinkle ridge profile calculated relative to the ends of each profile is consistent with previous estimates, which range from 0.03% to 0.8% [see review in 1]. Such values of horizontal strain, however, are sensitive to the profile width along which strain is calculated because strain localizes in proximity to faults [18]. Instead, the total energy released by faulting and folding within the area of the profile yields more widely applicable and meaningful results. Our solutions require a regional horizontal stress of 5.1 times lithostatic load (49.2 MPa/km) to drive both shear strain along the faults and strain within the surrounding crust. Evaluated within a 15 km deep profile at a unit width of 1 m, with 12 m of depth averaged model displacement of the profile ends (i.e. shortening), this is stress drop is equivalent to 253 TJ of total work done by faulting and folding along profile C–C'.

The ratio of maximum displacement (Dmax) to fault length (L) is a measure of the brittle strain accommodated across a wrinkle ridge (Fig. 1.2). The work done by this faulting is measured by the cumulative geologic moment, M_G, of the subjacent faults. M_G is the product of the average fault displacement, the effective shear modulus of the crust, and fault length & width [18]. Figure 1.3 shows the distribution of work done by faulting and the total work done by faulting & folding at each profile for a 1m wide along-strike section.

Implications: Our results reveal along-strike variability in M_G and present an innovative method of measuring wrinkle ridge segment lengths. Similar to displacement variations between two fractures linked along strike [19], overlaps between wrinkle ridge segments can be defined by along-strike M_G minima, such as at profile B–B'. The advantage of using M_G to define wrinkle ridge segment length is that traditional *displacement* minima techniques are most applicable to near-tip interactions between two fractures, but have ambiguous utility when applied to arrays of thrust-related folds (i.e. wrinkle ridges). M_G provides a measure of the effective along-strike length of the faults and folds comprising a wrinkle ridge segment. Isolating individual wrinkle ridge segments and quantifying their degree of interaction can be used to define temporal relationships between segments within a larger population, and ultimately the timing and origin of the causative stresses can be evaluated. Also, when integrated with fault population ages [20,21] or slip history, M_G yields moment release rates, equivalent to the power (in watts) accommodated by faulting, that can then be used to evaluate frictional heating and potential volatile release from adjacent permafrost, as well as map temporal variability in global heat flux.

References: [1] Schultz R.A. (2000) *JGR, 105,* 12035–12052. [2] Montési L.G. and Zuber M.T. (2000) *LPS XXXI,* Abs.1927. [3] Plescia J.B. (1991) *GRL, 18,* 913–916. [4] Golombek M.P. et al. (1991) *LPS XXI*, 679–693. [5] Watters T.R. and Robinson M.S. (1997) *JGR, 102,* 10889–10903. [6] Tate A. et al. (2002) *LPS XXXIII*, Abs.1828. [7] Mège D. and Reidel S.P. (2001) *GRL, 28*, 3545–3548. [8] Schultz R.A. and Aydin A. (1990) *Tectonics, 9*, 1387–1407. [9] Roering J.J. (1997) *JGR, 102,* 11901–11912. [10] Niño F. et al. (1998) *JSG, 20,* 503–516. [11] Okubo C.H. and Schultz R.A. (2002) *AGU Fall 2002*, Abs.T12G-01. [12] Schultz R.A. and Watters T.R. (2001) *GRL, 28,* 4659–4662. [13] Scott D.H. and Tanaka K.L. (1986) *USGS map* I-1802-A. [14] Hodges C.A. (1973) *NASA SP-330,* 31-12–31-12. [15] Lucchitta B.K. (1977) *LPS VIII*, 2691–2703. [16] Watters T.R. and Tuttle M.T. (1991) *LPS XXII*, 1477–1488. [17] Watters T.R. (1993) *JGR, 98*, 17049–17060. [18] Pollard D.D. and Segall P. (1987) *Fracture Mechanics of Rock*: Academic Press, 277–349. [19] Cartwright J.A. and Mansfield C.S. (1998) *JSG, 20*, 3–19. [20] Dohm, J.M., Tanaka, K.T., Hare, T.M. (2001) *USGS map* I-2650. [21] Wilkins et al. (2002) *GRL, 29*, doi:10.1029/2002GL015391.

Abstract published in: Lunar and Planetary Science XXXIV, CD-ROM, Lunar and Planetary Institute, Houston (2003).